10.1098/rspa.2000.0697

THE ROYAL SOCIETY

The onset of stationary Marangoni instability of an evaporating droplet

By Vai-Meng Ha and Chun-Liang Lai

Department of Mechanical Engineering, National Taiwan University, Taipei, Taiwan 106, Republic of China

Received 27 March 2000; accepted 9 October 2000

Evaporation at the surface of a liquid is an unsteady process involving heat and mass transport. The process of evaporation also leads to a local reduction in the temperature of the bulk liquid near the surface. Marangoni instability may then be induced by such a surface temperature reduction and the consequent variation in surface tension. The purpose of this study is to investigate theoretically the onset and physical mechanisms of Marangoni instability of an evaporating droplet. With the quasi-steady approximation, which means that the size change of the droplet is negligible, the surrounding gas motion is asymptotically steady and the temperature distribution of the droplet is temporarily frozen at each specified instant of interest, a lower limit of the onset condition for Marangoni instability is derived analytically through linear stability analysis. The following results are obtained from the analysis. As time proceeds, the temperature reduction and thermal boundary layer thickness near the free surface become larger and the droplet becomes more unstable. The critical wavenumber of small disturbances for the onset of Marangoni instability increases with the droplet initial temperature. The onset condition is a strong function of the droplet initial temperature with which the critical Marangoni number increases.

Keywords: Marangoni instability; evaporating droplet; linear stability anlyasis; quasi-steady approach

1. Introduction

With the availability of space laboratories, space platforms and space stations, more attention has been paid to the flow motions induced by surface tension gradients, which are usually overshadowed by the buoyancy force under terrestrial conditions.

The flow motion which is driven by surface tension gradient along the free surface or interface is called thermocapillary flow. Surface tension, in general, depends on temperature, concentration and electrical potential. The gradient of any one, or any combination, of those factors along the interface will lead to a surface tension gradient and might result in a flow motion immediately. However, in some cases, the gradients of those factors are perpendicular to the interface. A cellular flow motion might be generated only when a certain critical Marangoni number is exceeded. Such a flow phenomenon is called Marangoni instability, which becomes very crucial and interesting in microgravity researches both from the academic and application points of view.

A hexagonal flow pattern driven by the surface tension gradient, which had always been thought to be induced by the buoyancy effect, was first observed by Benard and was later justified experimentally and analytically by Block (1956) and Pearson (1958), respectively. Since then, many studies were directed to the understanding of the Marangoni instability in liquid layers with different boundary conditions. Sternling & Scriven (1959) have studied a similar situation arising from the mass transfer process between two immiscible liquid layers of large extent. They later returned to the work of Pearson (1958) and extended it by considering the effect of surface viscosity and surface deflexion (Scriven & Sternling 1964). Nield (1964) and Smith (1966) investigated both surface tension and buoyancy effects in a planar layer. Zeren & Reynolds (1972) considered the instability of two-liquid layers bounded by horizontal isothermal walls. Wahal & Bose (1988) predicted the instability of a two-layer problem heating from below through a rigid boundary and with a deformable free surface and a deformable liquid–liquid interface. Recently, in the planar layer, Ha (1998) and Ha & Lai (1998) investigated the Marangoni instability of an evaporating liquid layer. Similarity solutions were obtained prior to the onset of instability. Linear stability analysis was applied to obtain an analytical result for the onset Marangoni number.

In the meantime, considerable theoretical studies have been done on the stabilities of convective, especially unsteady, flows by the energy method (Davis 1969; Homsy 1973; Neitzel 1982; McTaggart 1984; Payne *et al.* 1988). In general, the variational principle is applied first for the formulation. Then a criterion for stability against disturbances of arbitrary amplitude is found. The linear perturbation theory and the energy method are complementary. Usually, the former gives the conditions above which the systems are definitely unstable (a lower bound of the unstable regime), while the latter gives the conditions under which the system are definitely stable (an upper bound of the stable regime).

Apart from planar flow, there are flow situations in which the curvature effect cannot be neglected. Hence much research has been devoted to theoretical studies with a cylindrical or a spherical geometry. The Marangoni instability of a liquid layer bounded by two coaxial cylinder surfaces has been investigated by Hoefsloot *et al.* (1990*a*). The instability of a droplet was first investigated by Chandrasekhar (1961). In recent years, Pirotte & Lebon (1988) investigated the Marangoni instability of a spherical liquid layer with an undeformable free surface. The critical Marangoni number obtained was higher than that for the planar case, which was considered mainly due to the existence of surface curvature. With an appropriate scaling analysis, their work was then corrected by Hoefsloot & Hoogstraten (1989). Since then, research has focused on problems of convection in a spherical shell heating from inner side (Hoefsloot *et al.* 1990*b*, 1992; Cloot & Lebon 1990*a*, *b*). Lebon *et al.* (1992) have reviewed some works in this problem. Wilson (1994), who extended the earlier work of Pirotte & Lebon (1988) and that of Hoefsloot & Hoogstraten (1989), and corrected the errors in the paper by Cloot & Lebon (1990*a*), investigated a similar problem with heating from either the inner or outer side. When heated from the outer side, the neutral curves were marked by the bifurcation when $Cr > \frac{1}{4}r_2$, where Cr is the Crispation number and r_2 is the dimensionless radius of the undisturbed outer free surface of the liquid. At such a condition, the system was unstable.

In addition to the above studies, Lozinski & Matalon (1993) performed analytical studies of spinning droplets with surface tension effects. Aharon & Shaw (1995, 1996)

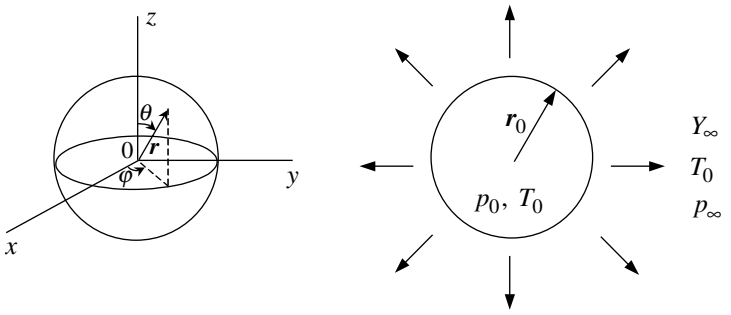

Figure 1. Schematic of the physical model and coordinate system.

investigated the Marangoni instability of a binary evaporating droplet with surface tension effects caused by both temperature and concentration gradients. Niazmand *et al.* (1995), Rednikov *et al.* (1995) and Shih & Megaridis (1996) studied vaporizing droplets that were moving relative to their environment.

In the present study, the instability of an evaporating droplet in a passive gas medium is investigated. Because of the evaporation, a temperature gradient near and perpendicular to the free surface is self-sustained. No external agency is needed to provide the temperature gradient. By the quasi-steady approximation (which means that the size change of the droplet is negligible and the surrounding gas motion is asymptotically steady), a lower limit of the onset condition for Marangoni instability with a temporarily frozen temperature distribution of the droplet is then obtained through linear stability analysis. The evaporation effect on the onset condition is also discussed.

2. Problem description

(*a*) *Evaporating process*

A motionless droplet of radius r_0 surrounded by a passive gas with an initial mass fraction Y_∞ of the liquid vapour and at temperature T_0 and pressure p_∞ is considered. The droplet is originally at temperature T_0 and pressure p_0 and with a constant evaporating rate at the surface. The schematic of the physical model is shown in figure 1.

When the droplet evaporates, it may absorb heat from its interior, which results in a temperature reduction near the surface. Meanwhile, a flow motion in the gas medium away from the droplet surface is generated. Conservation of mass, momentum and energy must be satisfied at the interface.

As the evaporation proceeds, the temperature reduction and the thermal boundary-layer thickness near the droplet surface become larger. It is this self-sustained and growing temperature reduction near the free surface and the consequent variation of surface tension that are the focus of the present study. We see how, as the evaporation proceeds and brings about the onset of Marangoni instability, a cellular flow motion may occur if the temperature reduction near the free surface is large enough such that the corresponding Marangoni number at that moment exceeds a certain critical value.

To illustrate the phenomena stated above, the temperature distributions for an octane droplet at different initial temperatures are shown in figure 2. Such tempera-

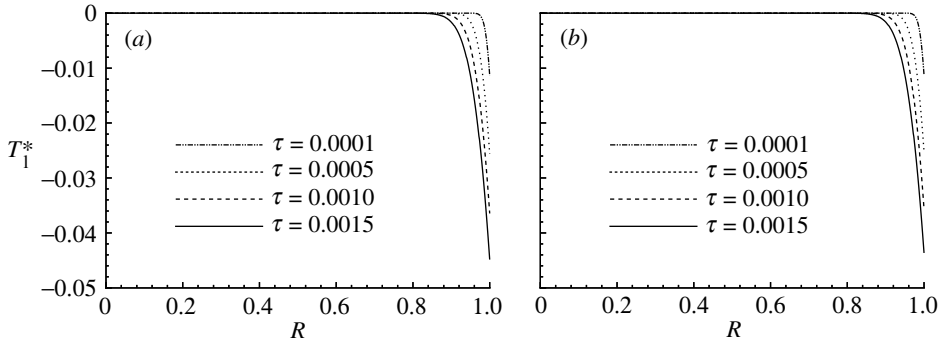

Figure 2. The dimensionless temperature distributions of an octane droplet at various instants for (*a*) $T_0 = 293$ K, (*b*) $T_0 = 353$ K.

Table 1. *Variation of surface temperature with time for an octane droplet at* $T_0 = 293$ K

dimensionless time τ	dimensional time t (s) for $r_0 = 5$ cm	dimensional time t (s) for $r_0 = 10$ cm	surface temperature T_s (K)	temperature drop ΔT_s (K)
0.0001	3.0	12.0	292.99	0.01
0.0005	15.0	60.0	292.98	0.02
0.001	30.0	120.0	292.97	0.03
0.0015	45.0	180.0	292.96	0.04

Table 2. *Variation of surface temperature with time for an octane droplet at* $T_0 = 353$ K

dimensionless time τ	dimensional time t (s) for $r_0 = 5$ cm	dimensional time t (s) for $r_0 = 10$ cm	surface temperature T_s (K)	temperature drop ΔT_s (K)
0.0001	3.5	14.0	352.73	0.27
0.0005	17.5	70.0	352.39	0.61
0.001	35.0	140.0	352.13	0.87
0.0015	52.5	210.0	351.93	1.07

ture distributions are obtained by solving the equations to be discussed in the next section. The temperature, length and time are scaled by $m_0' h_{lg} r_0/k_l$, r_0 and r_0^2/α_l, respectively, in which m_0' is the evaporation rate of droplet at the initial temperature T_0, h_{lg} is the heat of evaporation, k_l the liquid thermal conductivity and α_l the liquid thermal diffusivity. From figure 2, it is obvious that, as the evaporation proceeds, the surface temperature decreases and a thermal boundary layer is established near the free surface across which the temperature gradient is significant. For further illustration, the corresponding surface-temperature variations with time for an octane droplet are shown in tables 1 and 2. It can be seen that the surface-temperature decrease, ΔT_s, is a strong function of the initial temperature T_0. This is because the evaporation rate increases as the temperature approaches the boiling point.

Table 3. *Comparison of the various time-scales during evaporation*

(Based on data for octane and heptane from Daubert & Danner (1985): $\rho_l/\rho_g \sim O(10^3)$, $Pr_l \sim O(1 \sim 10)$, $\alpha_l/\alpha_g \sim O(10^{-2})$, $\mu_l/\mu_g \sim O(10^2)$, $Pr_g \sim 1$, $Le \sim 1$, $Re = A_0 r_0/\nu_g$ = radial Reynolds number $\sim O(1)$, A_0 = evaporating velocity at free surface.)

process	time-scale	time-scale with respect to r_0^2/α_l
gas phase flow	$\dfrac{r_0}{A_0}$	$\dfrac{\alpha_l}{A_0 r_0} = \dfrac{1}{RePr_l}\dfrac{\mu_l}{\mu_g}\dfrac{\rho_g}{\rho_l} \sim (10^{-2} \sim 10^{-1})$
transport in gas phase		
(a) diffusion of momentum	$\dfrac{r_0^2}{\nu_g}$	$\dfrac{\alpha_l}{\nu_g} = \dfrac{\alpha_l}{\alpha_g}\dfrac{1}{Pr_g} \sim 10^{-2}$
(b) diffusion of heat	$\dfrac{r_0^2}{\alpha_g}$	$\dfrac{\alpha_l}{\alpha_g} \sim 10^{-2}$
(c) diffusion of mass	$\dfrac{r_0^2}{D_g}$	$\dfrac{\alpha_l}{D_g} = \dfrac{\alpha_l}{\alpha_g} Le \sim 10^{-2}$
transport in liquid phase		
(a) diffusion of momentum	$\dfrac{r_0^2}{\nu_l}$	$\dfrac{\alpha_l}{\nu_l} = \dfrac{1}{Pr_l} \sim (10^{-1} \sim 1)$
(b) diffusion of heat	$\dfrac{r_0^2}{\alpha_l}$	1
droplet regression	$\dfrac{r_0}{\dot{r}_0} \simeq \dfrac{r_0\rho_l}{A_0\rho_g}$	$\dfrac{\alpha_l}{A_0 r_0}\dfrac{\rho_l}{\rho_g} = \dfrac{1}{RePr_l}\dfrac{\mu_l}{\mu_g} \sim (10 \sim 10^2)$

(*b*) *Quasi-steady approximation*

Strictly speaking, the evaporation of a droplet is never a steady process, since the radius, the surface temperature, and hence the evaporation rate, keep decreasing during the evaporation. However, as shown in table 3, the time-scales of the gas phase are two orders smaller than the time-scale of heat diffusion in the liquid phase. Therefore, when the interest is mainly on the liquid phase (the droplet), the gas phase (the surrounding air) can be treated as asymptotically steady. Nevertheless, the time-scale for the droplet regression is about one order larger than the heat diffusion time-scale of the droplet. Consequently, the size change of the droplet is neglected in the present study. This approximation will become more reasonable by choosing a larger size of droplet with a higher density ratio between the liquid phase and its vapour.

Because the temperature distribution of an evaporating droplet varies continuously, we cannot predict accurately the onset of a Marangoni instability of an evaporating droplet by a linear stability analysis without considering the time-evolution effect (Homsy 1973). There have been several important research papers regarding the instability of a time-dependent basic state. To describe the growth and evolution of small disturbances with time-dependent flows, a nonlinear analysis of finite-amplitude instability is necessary (Davis 1970). To predict the onset condition and onset time of instability of a time-dependent basic state, the energy method is an appropriate approach (Davis 1969; Homsy 1973; Neitzel 1982), which gives a sufficient condition for stability against disturbances. To treat the growth of small disturbances as an initial problem is another approach, in which the time evolu-

tion of the initial disturbances is monitored by numerically integrating the unsteady perturbation equations (Mahler *et al.* 1968; Chen & Kirchner 1971). However, a major difficulty with this method is the choice of initial conditions. Although it is inappropriate for marginal instability and usually underestimates the onset time for instability (Homsy 1973), the quasi-steady approach, in which the stability of a 'frozen' basic state is analysed, is still applied to give a sufficient condition of instability and obtain certain essential physics (Chen & Kirchner 1971; Kerr 1989). Conceptually, the quasi-steady approach indicates, in a sense, the 'driving potential' of each instantaneous basic state for the onset of instability, if it remains long enough. If the time-dependent basic state becomes suppressive as time proceeds, the quasi-steady approach will not be able to provide any useful information. However, if it is always conducive to the onset of stability over time, according to the present study, such an approach could be useful in predicting the condition sufficient sufficient for the onset of Marangoni instability. Therefore, as a first approach to such a difficult and complicated problem to acquire some basic and essential physics for the onset of Marangoni instability of an evaporating droplet, a linear stability analysis with a temporarily 'frozen' temperature distribution of the droplet is employed in the present study. The onset condition for the neutral instability is calculated to provide a sufficient condition for the onset of Marangoni instability which will be discussed in detail when the results are presented. Moreover, with such an approximation, the expression for the onset Marangoni number of instability can be obtained analytically (equation (4.31)) to provide a clear and direct understanding of the physical mechanisms for the onset of instability. With such an understanding, any further study involving the time evolution of small disturbances, along with the unsteady temperature variation of the droplet, will become more productive.

In summary, the quasi-steady approximation used in the present study is as follows.

(1) The transport phenomena of the surrounding gas phase are treated as steady state.

(2) The regression of the droplet during evaporation is negligibly small.

(3) The temperature distribution of the droplet is temporarily frozen at certain specified instants with an application of linear stability analysis.

3. Quasi-steady analysis

Apart from the quasi-steady approximation, the following assumptions are made for further simplification of the problem.

(1) The free surface is undeformable. As a result, the Gibbs–Thomson effect is not important in the present study.

(2) The buoyancy effect is neglected under the microgravity condition.

(3) All the physical properties of the fluid (except the surface tension, which is a monotonically decreasing function of the temperature) are considered to be constant.

(4) Viscous dissipation and radiative heat transfer are neglected.

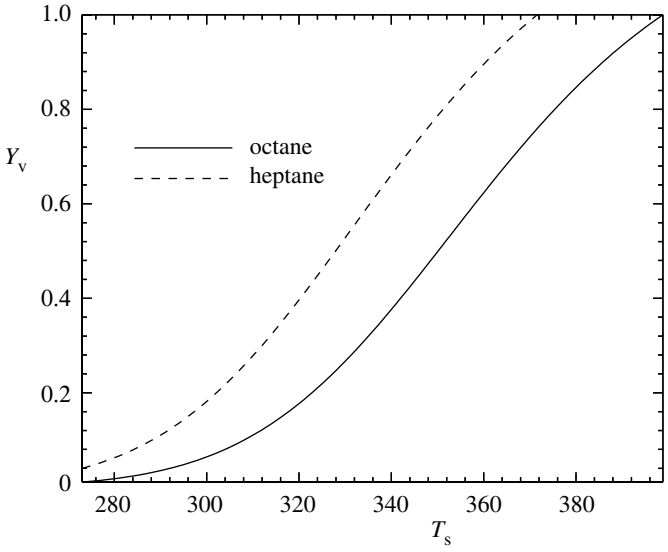

Figure 3. Mass fraction of the liquid vapour at the free surface of an octane and a heptane droplet for various initial temperatures.

(5) The liquid vapour is saturated at the droplet surface. An independent relation between the surface temperature T_s and the mass fraction of liquid vapour Y_v, i.e. the Clausius–Clapeyron equation (Gogos & Ayyaswamy 1988), is

$$Y_v(r_0) = \frac{\exp[(h_{lg}/\Re)(1/T_b - 1/T_s)]}{r_w - (r_w - 1)\exp[(h_{lg}/\Re)(1/T_b - 1/T_s)]}. \tag{3.1}$$

In the above expression, T_b is the boiling temperature of liquid, $\Re$ is the universal gas constant and r_w is the ratio of molecular weights M_{amb}/M_l. Y_v is a function of the physical properties of the fluid h_{lg}, T_b and r_w. In figure 3, Y_v is plotted against the surface temperature T_s for heptane and octane. It increases with temperature and varies from 0 to 1. The limit zero corresponds to a non-evaporating situation and $Y_v = 1$ corresponds to the boiling state. Heptane, which has a lower boiling point, possesses a higher mass fraction at a given temperature.

With the quasi-steady approximation and the above assumptions, the governing equations of the system are

$$\nabla \cdot \boldsymbol{V}_g = 0, \tag{3.2}$$

$$\nabla \cdot \boldsymbol{V}_l = 0, \tag{3.3}$$

$$\rho_g \boldsymbol{V}_g \cdot \nabla \boldsymbol{V}_g = -\nabla p_g + \mu_g \nabla^2 \boldsymbol{V}_g, \tag{3.4}$$

$$\rho_l \left(\frac{\partial \boldsymbol{V}_l}{\partial t} + \boldsymbol{V}_l \cdot \nabla \boldsymbol{V}_l \right) = -\nabla p_l + \mu_l \nabla^2 \boldsymbol{V}_l, \tag{3.5}$$

$$\boldsymbol{V}_g \cdot \nabla T_g = \alpha_g \nabla^2 T_g, \tag{3.6}$$

$$\frac{\partial T_l}{\partial t} + \boldsymbol{V}_l \cdot \nabla T_l = \alpha_l \nabla^2 T_l, \tag{3.7}$$

$$\boldsymbol{V}_g \cdot \nabla Y_v = D_g \nabla^2 Y_v, \tag{3.8}$$

where $\boldsymbol{V}(u_\mathrm{r}, u_\theta, u_\phi)$ is the velocity vector, with u_r, u_θ and u_ϕ being the velocity components in the r-, θ- and ϕ-directions. T is the temperature, p denotes the pressure, Y_v is the mass fraction of liquid vapour, ρ is the density, μ is the viscosity, α denotes the thermal diffusivity, D is the mass diffusivity and t is time. The subscript 'g' refers to the gas phase and 'l' refers to the liquid phase.

For the convenience and generality of the analysis and discussion, the variables are non-dimensionalized. The scaling factors for r, t, $\boldsymbol{V}$, p and Y_v are r_0, r_0^2/α_l, α_l/r_0, $\rho_\mathrm{l}\alpha_\mathrm{l}^2/r_0^2$ and Y_0, respectively. Y_0 is the initial mass fraction of the liquid vapour at the free surface. By further defining

$$\left.\begin{gathered} T_\mathrm{l}^* = \frac{T_\mathrm{l} - T_0}{m_0' h_\mathrm{lg} r_0/k_\mathrm{l}}, \qquad T_\mathrm{g}^* = \frac{T_\mathrm{g} - T_0}{m_0' h_\mathrm{lg} r_0/k_\mathrm{l}}, \\ \phi_{Cp} = \frac{Cp_\mathrm{l}}{Cp_\mathrm{g}}, \qquad \phi_k = \frac{k_\mathrm{l}}{k_\mathrm{g}}, \qquad \phi_\alpha = \frac{\alpha_\mathrm{l}}{\alpha_\mathrm{g}}, \qquad \phi_\mu = \frac{\mu_\mathrm{l}}{\mu_\mathrm{g}}, \\ \phi_\rho = \frac{\rho_\mathrm{l}}{\rho_\mathrm{g}}, \qquad Cr = \frac{\mu_\mathrm{l}\alpha_\mathrm{l}}{\sigma_0 r_0}, \qquad Le = \frac{\alpha_\mathrm{g}}{D_\mathrm{g}}, \qquad Pr_\mathrm{l} = \frac{\nu_\mathrm{l}}{\alpha_\mathrm{l}}, \qquad Pr_\mathrm{g} = \frac{\nu_\mathrm{g}}{\alpha_\mathrm{g}}, \end{gathered}\right\} \tag{3.9}$$

the dimensionless governing equations possess the following forms:

$$\nabla \cdot \boldsymbol{V}_\mathrm{g}^* = 0, \tag{3.10}$$

$$\nabla \cdot \boldsymbol{V}_\mathrm{l}^* = 0, \tag{3.11}$$

$$\frac{\phi_\alpha}{Pr_\mathrm{g}}\left(\boldsymbol{V}_\mathrm{g}^* \cdot \nabla \boldsymbol{V}_\mathrm{g}^* + \phi_\rho \nabla p_\mathrm{g}^*\right) = \nabla^2 \boldsymbol{V}_\mathrm{g}^*, \tag{3.12}$$

$$\frac{1}{Pr_\mathrm{l}}\left(\frac{\partial \boldsymbol{V}_\mathrm{l}^*}{\partial \tau} + \boldsymbol{V}_\mathrm{l}^* \cdot \nabla \boldsymbol{V}_\mathrm{l}^* + \nabla p_\mathrm{l}^*\right) = \nabla^2 \boldsymbol{V}_\mathrm{l}^*, \tag{3.13}$$

$$\phi_\alpha \boldsymbol{V}_\mathrm{g}^* \cdot \nabla T_\mathrm{g}^* = \nabla^2 T_\mathrm{g}^*, \tag{3.14}$$

$$\frac{\partial T_\mathrm{l}^*}{\partial \tau} + \boldsymbol{V}_\mathrm{l}^* \cdot \nabla T_\mathrm{l}^* = \nabla^2 T_\mathrm{l}^*, \tag{3.15}$$

$$\phi_\alpha Le \boldsymbol{V}_\mathrm{g}^* \cdot \nabla Y_\mathrm{v}^* = \nabla^2 Y_\mathrm{v}^*. \tag{3.16}$$

The relevant initial and boundary conditions are as follows.

The initial conditions at $\tau = 0$ are

$$\boldsymbol{V}_\mathrm{l}^* = 0, \tag{3.17}$$

$$T_\mathrm{l}^* = 0. \tag{3.18}$$

The boundary conditions as $R \to \infty$ are

$$\boldsymbol{V}_\mathrm{g}^* = 0, \tag{3.19}$$

$$T_\mathrm{g}^* = 0, \tag{3.20}$$

$$p_\mathrm{g}^* = p_\infty^*, \tag{3.21}$$

$$Y_\mathrm{v}^* = Y_\infty^* = 0. \tag{3.22}$$

The boundary conditions at the centre of the droplet ($R = 0$) are

$$\boldsymbol{V}_\mathrm{l}^* = 0, \tag{3.23}$$

$$T_\mathrm{l}^* = \text{finite}. \tag{3.24}$$

At the interface $R = 1$, the continuity of tangential velocity, mass flux, stresses, temperature and heat flux and the non-condensible condition of the passive gas must be satisfied, which gives

$$u^*_{\theta,\mathrm{l}} = u^*_{\theta,\mathrm{g}}, \tag{3.25}$$

$$u^*_{\phi,\mathrm{l}} = u^*_{\phi,\mathrm{g}}, \tag{3.26}$$

$$\phi_\rho(u^*_{R,\mathrm{l}} - \dot{R}) = u^*_{R,\mathrm{g}} - \dot{R} = Ev, \tag{3.27}$$

$$\phi_\mu\left[R\frac{\partial}{\partial R}\left(\frac{u^*_{\theta,\mathrm{l}}}{R}\right) + \frac{1}{R}\frac{\partial u^*_{R,\mathrm{l}}}{\partial\theta}\right] - \left[R\frac{\partial}{\partial R}\left(\frac{u^*_{\theta,\mathrm{g}}}{R}\right) + \frac{1}{R}\frac{\partial u^*_{R,\mathrm{g}}}{\partial\theta}\right] = -\phi_\mu\frac{Ma}{R}\frac{\partial T^*_{\mathrm{l}}}{\partial\theta}, \tag{3.28}$$

$$\phi_\mu\left[\frac{1}{R\sin\theta}\frac{\partial u^*_{R,\mathrm{l}}}{\partial\phi} + R\frac{\partial}{\partial R}\left(\frac{u^*_{\phi,\mathrm{l}}}{R}\right)\right] - \left[\frac{1}{R\sin\theta}\frac{\partial u^*_{R,\mathrm{g}}}{\partial\phi} + R\frac{\partial}{\partial R}\left(\frac{u^*_{\phi,\mathrm{g}}}{R}\right)\right] = -\phi_\mu\frac{Ma}{R\sin\theta}\frac{\partial T^*_{\mathrm{l}}}{\partial\phi}, \tag{3.29}$$

$$\left(-p^*_{\mathrm{l}} + 2Pr_{\mathrm{l}}\frac{\partial u^*_{R,\mathrm{l}}}{\partial R}\right) - \left(-p^*_{\mathrm{g}} + \frac{2Pr_{\mathrm{g}}}{\phi_\alpha\phi_\rho}\frac{\partial u^*_{R,\mathrm{g}}}{\partial R}\right) = -2\frac{Pr_{\mathrm{l}}}{Cr}, \tag{3.30}$$

$$T^*_{\mathrm{g}} = T^*_{\mathrm{l}} = T^*_{\mathrm{s}}, \tag{3.31}$$

$$-\frac{\partial T^*_{\mathrm{l}}}{\partial R} = -\frac{1}{\phi_k}\frac{\partial T^*_{\mathrm{g}}}{\partial R} + \frac{m'}{m'_0}, \tag{3.32}$$

$$\frac{1}{\phi_\alpha Le}\frac{\partial Y^*_{\mathrm{v}}}{\partial R} = -\left(\frac{1}{Y_0} - Y^*_{\mathrm{v}}\right)u^*_{R,\mathrm{g}}, \tag{3.33}$$

where $\dot{R}$ is the regression rate of the droplet to be neglected in the later analysis under the quasi-steady approximation and $Ev = m'/(\rho_{\mathrm{l}}\alpha_{\mathrm{l}}/r_0)$ is the dimensionless evaporating mass per unit area per unit time at the free surface. The expression for Ev will be obtained later by using the velocity field of the gas phase. The Marangoni number is

$$Ma = -\frac{\partial\sigma}{\partial T}\frac{m'_0 h_{\mathrm{lg}} r_0^2}{\mu_{\mathrm{l}}\alpha_{\mathrm{l}}k_{\mathrm{l}}}.$$

The mass fraction at the droplet surface $Y^*_{\mathrm{v}}(1)$ is calculated by the Clausius–Clapeyron equation.

Although the temperature distribution of the droplet changes constantly as the evaporation proceeds, there would be no fluid motion generated inside the droplet if the evaporation is uniform over the free surface and no any disturbance exists, i.e. $\boldsymbol{V}^*_{\mathrm{l}} = 0$. The pressure of the droplet is then constant and static in nature and can be determined by the following normal-force balance condition at the surface:

$$p^*_{\mathrm{l}} = p^*_{\mathrm{g}} - \frac{2Pr_{\mathrm{g}}}{\phi_\alpha\phi_\rho}\frac{\partial u^*_{R,\mathrm{g}}}{\partial R} + \frac{2Pr_{\mathrm{l}}}{Cr}. \tag{3.34}$$

However, the evaporation will result in an outward flow motion away from the droplet surface in the gas phase. The governing equations for such a radial gas flow are as

follows:

$$\frac{1}{R^2}\frac{\partial}{\partial R}(R^2 u^*_{R,\mathrm{g}}) = 0, \tag{3.35}$$

$$\frac{\phi_\alpha}{Pr_\mathrm{g}}\left(u^*_{R,\mathrm{g}}\frac{\partial u^*_{R,\mathrm{g}}}{\partial R} + \phi_\rho\frac{\partial p^*_\mathrm{g}}{\partial R}\right) = \frac{1}{R^2}\frac{\partial}{\partial R}\left(R^2\frac{\partial u^*_{R,\mathrm{g}}}{\partial R}\right) - \frac{2u^*_{R,\mathrm{g}}}{R^2}, \tag{3.36}$$

$$\phi_\alpha u^*_{R,\mathrm{g}}\frac{\partial T^*_\mathrm{g}}{\partial R} = \frac{1}{R^2}\frac{\partial}{\partial R}\left(R^2\frac{\partial T^*_\mathrm{g}}{\partial R}\right), \tag{3.37}$$

$$\phi_\alpha Le u^*_{R,\mathrm{g}}\frac{\partial Y^*_\mathrm{v}}{\partial R} = \frac{1}{R^2}\frac{\partial}{\partial R}\left(R^2\frac{\partial Y^*_\mathrm{v}}{\partial R}\right). \tag{3.38}$$

Solved with the corresponding boundary conditions as shown in equations (3.19)–(3.22), (3.25)–(3.27), (3.31) and (3.33), the radial velocity, pressure, temperature and liquid vapour distributions of the surrounding gas can then be determined analytically. They are

$$u^*_{R,\mathrm{g}} = -\frac{\ln(1-Y_\mathrm{v}(1))}{\phi_\alpha Le}\frac{1}{R^2}, \tag{3.39}$$

$$p^*_\mathrm{g} = -\frac{\ln^2(1-Y_\mathrm{v}(1))}{\phi^2_\alpha\phi_\rho Le^2}\frac{1}{2R^4} + p^*_\infty, \tag{3.40}$$

$$T^*_\mathrm{g} = T^*_\mathrm{s}\frac{(1-Y_\mathrm{v}(1))^{1/(Le\cdot R)} - 1}{(1-Y_\mathrm{v}(1))^{1/Le} - 1}, \tag{3.41}$$

$$Y^*_\mathrm{v} = \frac{1}{Y_0}\left[1 - (1-Y_\mathrm{v}(1))^{1/R}\right], \tag{3.42}$$

where

$$Y_\mathrm{v}(1) = \frac{\exp[(h_\mathrm{fg}/\Re)(1/T_\mathrm{b} - 1/T_\mathrm{s})]}{r_\mathrm{w} - (r_\mathrm{w}-1)\exp[(h_\mathrm{fg}/\Re)(1/T_\mathrm{b} - 1/T_\mathrm{s})]}. \tag{3.43}$$

p^*_l can now be determined from equations (3.39) and (3.40):

$$p^*_\mathrm{l} = \frac{2Pr_\mathrm{l}}{Cr} - \frac{4Pr_\mathrm{g}}{\phi^2_\alpha\phi_\rho Le}\ln(1-Y_\mathrm{v}(1)) - \frac{1}{2\phi_\rho\phi^2_\alpha Le^2}\ln^2(1-Y_\mathrm{v}(1)) + p^*_\infty. \tag{3.44}$$

The temperature field of the droplet, $T^*_\mathrm{l}(R,\tau)$, cannot be solved easily in an analytic form and has to be determined from the following energy equation and conditions:

$$\frac{\partial T^*_\mathrm{l}}{\partial\tau} = \frac{1}{R^2}\frac{\partial}{\partial R}\left(R^2\frac{\partial T^*_\mathrm{l}}{\partial R}\right), \tag{3.45}$$

$$T^*_\mathrm{l} = 0 \quad \text{for } \tau = 0, \tag{3.46}$$

$$T^*_\mathrm{l} = \text{finite} \quad \text{for } R = 0, \tag{3.47}$$

$$-\frac{\partial T^*_\mathrm{l}}{\partial R} = T^*_\mathrm{s}Bi + Rm \quad \text{for } R = 1. \tag{3.48}$$

In (3.48), the first term of the right-hand side represents the heat transfer to the ambient by convection and the second term denotes the heat flux due to evaporation

at the free surface, with the parameters defined as

$$Bi = \frac{1}{\phi_k Le} \ln(1 - Y_{\rm v}(1)) \frac{(1 - Y_{\rm v}(1))^{1/Le}}{(1 - Y_{\rm v}(1))^{1/Le} - 1}, \tag{3.49}$$

$$Rm = \frac{m'}{m'_0} = \frac{\ln(1 - Y_{\rm v}(1))}{\ln(1 - Y_0(1))}. \tag{3.50}$$

The transient temperature distributions of the droplet are solved numerically by using Crank–Nicolson method and are calculated for several specified instants, as shown in figure 2. All the physical variables of the gas phase which are expressed in terms of the surface temperature $T_{\rm s}^*$ can then be determined.

4. Stability analysis

(*a*) *Perturbed equations*

Suppose the surface temperature is perturbed due to either a non-uniform evaporation or other reasons, and a local thermocapillary convection due to Marangoni effect is generated through boundary conditions (3.28) and (3.29). The concern is whether such disturbances will be amplified or damped. As discussed in § 2, a linear stability analysis with a frozen temperature distribution of the droplet for each specified instant of interest is employed in the present study to investigate the onset of Marangoni instability. With the quasi-steady approximation, the effect on the Marangoni convection in the droplet due to the surrounding atmosphere is directly through the thermal and mass boundary conditions on the interface.

To determine the onset of instability, situations with infinitesimal disturbances on the basic flow in the liquid phase are considered in this section. In the following analysis, a prime will be used to denote the perturbed quantities and, for simplification, the subscript 'l', previously used for the liquid phase, is to be neglected. The linearized dimensionless equations for the perturbed quantities then become

$$\nabla \cdot \boldsymbol{V}' = 0, \tag{4.1}$$

$$\left(\nabla^2 - \frac{1}{Pr}\frac{\partial}{\partial \tau}\right)\boldsymbol{V}' = \frac{1}{Pr}\nabla p', \tag{4.2}$$

$$\left(\nabla^2 - \frac{\partial}{\partial \tau}\right)T' = u'_R \frac{\partial T^*}{\partial R}. \tag{4.3}$$

The corresponding boundary conditions are, for $R = 0$,

$$\boldsymbol{V}' = 0, \tag{4.4}$$

$$T' = \text{finite}, \tag{4.5}$$

and, for $R = 1$,

$$\phi_\rho u'_R = \frac{{\rm d}Ev}{{\rm d}T^*} T', \tag{4.6}$$

$$R\frac{\partial}{\partial R}\left(\frac{u'_\theta}{R}\right) + \frac{1}{R}\frac{\partial u'_R}{\partial \theta} = -\frac{Ma}{R}\frac{\partial T'}{\partial \theta}, \tag{4.7}$$

$$\frac{1}{R\sin\theta}\frac{\partial u'_R}{\partial\phi} + R\frac{\partial}{\partial R}\left(\frac{u'_\phi}{R}\right) = -\frac{Ma}{R\sin\theta}\frac{\partial T'}{\partial\phi}, \tag{4.8}$$

$$-\frac{\partial T'}{\partial R} = \left(Bi + \frac{\mathrm{d}Bi}{\mathrm{d}T^*}T^* + \frac{\mathrm{d}Rm}{\mathrm{d}T^*}\right)T', \tag{4.9}$$

where

$$Ev = -\frac{1}{\phi_\alpha Le}\frac{\phi_\rho}{\phi_\rho - 1}\ln(1 - Y_\mathrm{v}(1)). \tag{4.10}$$

To eliminate p', we take the curl of (4.2) twice and the radial component satisfies the following equation:

$$\nabla^2\left[\nabla^2 - \frac{1}{Pr}\frac{\partial}{\partial\tau}\right](Ru'_R) = 0. \tag{4.11}$$

With the continuity equation, we can combine the two tangential-stress boundary conditions into a single one, i.e.

$$\frac{\partial^2}{\partial R^2}(Ru'_R) - \frac{(2+L^2)(Ru'_R)}{R^2} = \frac{Ma}{R}L^2T', \tag{4.12}$$

where

$$\begin{aligned} L^2 &= \frac{1}{\sin\theta}\frac{\partial}{\partial\theta}\left(\sin\theta\frac{\partial}{\partial\theta}\right) + \frac{1}{\sin^2\theta}\frac{\partial^2}{\partial\phi^2} \\ &= R^2\nabla^2 - \frac{\partial}{\partial R}\left(R^2\frac{\partial}{\partial R}\right). \end{aligned} \tag{4.13}$$

Motivated by the operator L^2, the perturbed quantities are expressed in terms of spherical harmonics. Accordingly, we write

$$\left.\begin{aligned} Ru'_R &= U(R)Y_l^m(\theta,\phi)\mathrm{e}^{\omega\tau}, \\ T' &= \Im(R)Y_l^m(\theta,\phi)\mathrm{e}^{\omega\tau}, \end{aligned}\right\} \tag{4.14}$$

with ω being a complex quantity, i.e.

$$\omega = \omega_\mathrm{r} + \mathrm{i}\omega_\mathrm{i}. \tag{4.15}$$

The real part ω_r determines the degree of amplification or damping whereas the imaginary part ω_i is the circular frequency of disturbances. The spherical harmonics Y_l^m satisfies the following equation:

$$\left[\frac{1}{\sin\theta}\frac{\partial}{\partial\theta}\left(\sin\theta\frac{\partial}{\partial\theta}\right) + \frac{1}{\sin^2\theta}\frac{\partial^2}{\partial\phi^2}\right]Y_l^m(\theta,\phi) = -l(l+1)Y_l^m(\theta,\phi), \tag{4.16}$$

where

$$Y_l^m(\theta,\phi) = P_l^m(\cos\theta)\mathrm{e}^{\mathrm{i}m\phi}, \tag{4.17}$$

with $P_l^m(\cos\theta)$ being the associated Legendre polynomials.

Substitution of the solutions given in (4.14) into (4.1), (4.3) and (4.11) and boundary conditions (4.4)–(4.6), (4.9) and (4.12) gives

$$\left[\frac{\mathrm{d}^2}{\mathrm{d}R^2}+\frac{2}{R}\frac{\mathrm{d}}{\mathrm{d}R}-\frac{l(l+1)}{R^2}\right]\left[\frac{\mathrm{d}^2}{\mathrm{d}R^2}+\frac{2}{R}\frac{\mathrm{d}}{\mathrm{d}R}-\frac{l(l+1)}{R^2}-\frac{\omega}{Pr}\right]U=0, \tag{4.18}$$

$$\left[\frac{\mathrm{d}^2}{\mathrm{d}R^2}+\frac{2}{R}\frac{\mathrm{d}}{\mathrm{d}R}-\frac{l(l+1)}{R^2}-\omega\right]\Im-\frac{U}{R}\frac{\partial T^*}{\partial R}=0, \tag{4.19}$$

$$U=0 \quad \text{for } R=0, \tag{4.20}$$

$$\Im=\text{finite} \quad \text{for } R=0, \tag{4.21}$$

$$\phi_\rho\frac{U}{R}=\frac{\mathrm{d}Ev}{\mathrm{d}T^*}\Im \quad \text{for } R=1, \tag{4.22}$$

$$\frac{\mathrm{d}^2U}{\mathrm{d}R^2}-\frac{2-l(l+1)}{R^2}U=-Ma\frac{l(l+1)}{R}\Im, \tag{4.23}$$

$$-\frac{\mathrm{d}\Im}{\mathrm{d}R}=\left(Bi+\frac{\mathrm{d}Bi}{\mathrm{d}T^*}T^*+\frac{\mathrm{d}Rm}{\mathrm{d}T^*}\right)\Im=\chi\Im, \tag{4.24}$$

where

$$\chi=\left(Bi+\frac{\mathrm{d}Bi}{\mathrm{d}T^*}T^*+\frac{\mathrm{d}Rm}{\mathrm{d}T^*}\right),$$

a parameter indicating the heat transfer to the surrounding gas phase during the evaporation process.

Hence the instability problem is reduced to an eigenvalue problem of (4.18), (4.19) with boundary conditions (4.20)–(4.24).

Since the temperature distribution of the droplet is temporarily frozen in the above formulation, the analysis is valid for small disturbances with finite growth rate, $\omega_\mathrm{r} > O(1)$. However, the criterion of marginal or neutral instability ($\omega_\mathrm{r}=0$) is derived in the next section purposely to provide a sufficient condition for the onset of Marangoni instability. Moreover, the expression for the onset Marangoni number of neutral instability can be derived analytically, which provides a clear and direct understanding of the physical mechanism for the onset of instability.

(*b*) *Criterion of neutral instability*

It will be assumed here that the principle of exchange of stabilities holds, that is, if $\omega_\mathrm{r}=0$, then $\omega_\mathrm{i}=0$ automatically. The instability then appears as stationary, rather than oscillatory. For certain convective motion, induced solely by surface tension, such a principle was proved by Vidal & Acrivos (1966). Therefore, in this section, ω is put equal to zero. The onset Marangoni number for the frozen temperature distribution at a specified instant τ is then determined as a function of the wavenumber l with parameters Bi, Rm and Ev prescribed.

By setting $\omega=0$, the eigenvalue problem is simplified to

$$\left[\frac{\mathrm{d}^2}{\mathrm{d}R^2}+\frac{2}{R}\frac{\mathrm{d}}{\mathrm{d}R}-\frac{l(l+1)}{R^2}\right]^2U=0, \tag{4.25}$$

$$\left[\frac{\mathrm{d}^2}{\mathrm{d}R^2}+\frac{2}{R}\frac{\mathrm{d}}{\mathrm{d}R}-\frac{l(l+1)}{R^2}\right]\Im-\frac{U}{R}\frac{\partial T^*}{\partial R}=0, \tag{4.26}$$

together with boundary conditions (4.20)–(4.24). The solution of (4.25), with boundary condition (4.20), is

$$U(R) = A(R^l - aR^{l+2}). \tag{4.27}$$

Although the constant A, whose value depends on the amplitude of initial disturbances, is arbitrary, it drops out in the determination of the onset Marangoni number of instability (Dijkstra & van de Vooren 1985). The constant a is determined from (4.22), the continuity of mass flux at the free surface.

With the above velocity distribution, the solution of (4.26) subject to conditions (4.21) and (4.24) is

$$\Im(R) = BR^l - A\frac{R^{-(l+1)}}{2l+1}\int_0^R (s^{2l+1} - as^{2l+3})\frac{\partial T^*}{\partial s}\,\mathrm{d}s + A\frac{R^l}{2l+1}\int_0^R (1 - as^2)\frac{\partial T^*}{\partial s}\,\mathrm{d}s, \tag{4.28}$$

where

$$B = -A\int_0^1 (R^{2l+1} - aR^{2l+3})\frac{\partial T^*}{\partial R}\,\mathrm{d}R \cdot \frac{l+1-\chi}{(2l+1)(l+\chi)} - A\int_0^1 (1 - aR^2)\frac{\partial T^*}{\partial R}\,\mathrm{d}R \cdot \frac{1}{2l+1}. \tag{4.29}$$

From condition (4.22), the constant a is then determined as

$$a = \left[(l+\chi) + \frac{\mathrm{d}Ev}{\mathrm{d}T^*}\int_0^1 R^{2l+1}\frac{\partial T^*}{\partial R}\,\mathrm{d}R\right] \Big/ \left[(l+\chi) + \frac{\mathrm{d}Ev}{\mathrm{d}T^*}\int_0^1 R^{2l+3}\frac{\partial T^*}{\partial R}\,\mathrm{d}R\right]. \tag{4.30}$$

With the perturbed velocity and temperature fields as determined by (4.27), (4.28), the onset Marangoni number for the stationary instability can now be solved, i.e.

$$Ma = -\frac{2(l+\chi)[a(l^2+2l) - l^2 + 1]}{l(l+1)\bar{T}}, \tag{4.31}$$

with

$$\bar{T} = \int_0^1 (R^{2l+1} - aR^{2l+3})\frac{\partial T^*}{\partial R}\,\mathrm{d}R, \tag{4.32}$$

an expression implying, in a sense, the temperature reduction near the free surface due to evaporation. From (4.31), it is obvious that Ma increases with χ and decreases with $|\bar{T}|$.

5. Results and discussion

Results for an octane droplet will be presented and discussed in this section. Similar results were obtained for a heptane droplet. The values of the physical properties of octane and heptane are given by Daubert & Danner (1985).

Although there is no principle of exchange of stabilities for $\omega_\mathrm{r} \neq 0$ as for the case of marginal or neutral instability, the numerical calculations indicate that, without surface deformation, only the stationary instability, i.e. $\omega_\mathrm{i} = 0$, is possible for an

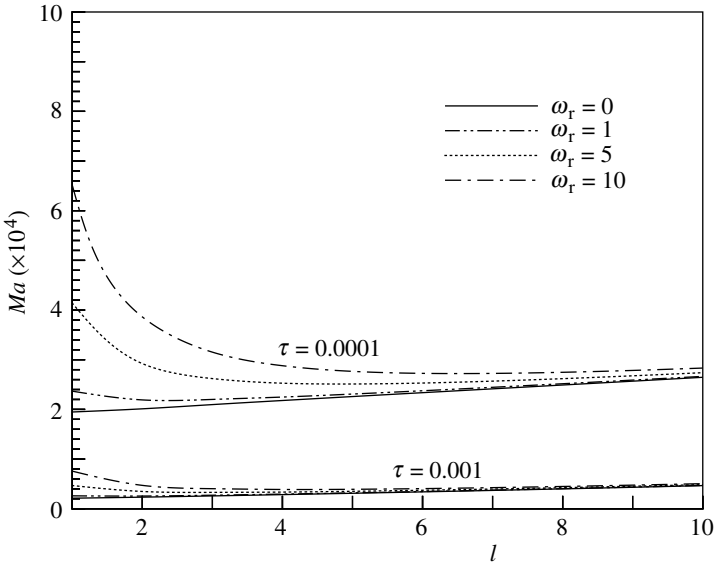

Figure 4. Onset Marangoni number versus disturbance wavenumber with different growth rates for a non-deformable octane droplet at $T_0 = 293$ K and two time instants.

evaporating droplet with different disturbance growth rates. Therefore, the stationary mode is implied wherever the onset of Marangoni instability is discussed in the following.

Shown in figure 4 are the variations of the onset Marangoni number as a function of the disturbance wavenumber for an octane droplet at an initial temperature $T_0 = 293$ K and four specified growth rates. Results obtained for the droplet temperature distributions at two different instants, i.e. $\tau = 0.0001$ and 0.001, are presented for comparison. Curves with $\omega_r = 0$ denote the neutral or marginal instability, while the ones with $\omega_r = 1$ and 5 are instability curves when the time-scale of the disturbance growth and that of the droplet temperature variation are of the same order of magnitude. Curves with $\omega_r = 10$ represent, as an example, a situation when the linear stability analysis with a temporarily frozen temperature distribution of the droplet is a good approximation. When $\omega_r = 0$, 1 and 5, the time evolution of the droplet temperature distribution is essential to the disturbance growth. However, as discussed in § 2, since the temperature reduction near the droplet surface becomes larger and larger, which is more and more conducive to the onset of Marangoni instability as time proceeds and evaporation continues, the linear stability analysis with a temporarily frozen temperature distribution provides, therefore, a sufficient condition for the onset of instability.

It can be found from figure 4 that, at each specific instant, the onset Marangoni number increases with the disturbance growth rate. As a result, the critical Marangoni number, Ma_c, which is defined as the smallest value of each instability curve, and the corresponding critical wavenumber, l_c, also increase with the disturbance growth rate. Variations of Ma_c as a function of ω_r for $\tau = 0.0001$ and 0.001, with the corresponding l_c, are shown in figure 5. Although the corresponding critical wavenumbers are different, the critical Marangoni number for different disturbance growth rates are about the same order of magnitude. Moreover, such

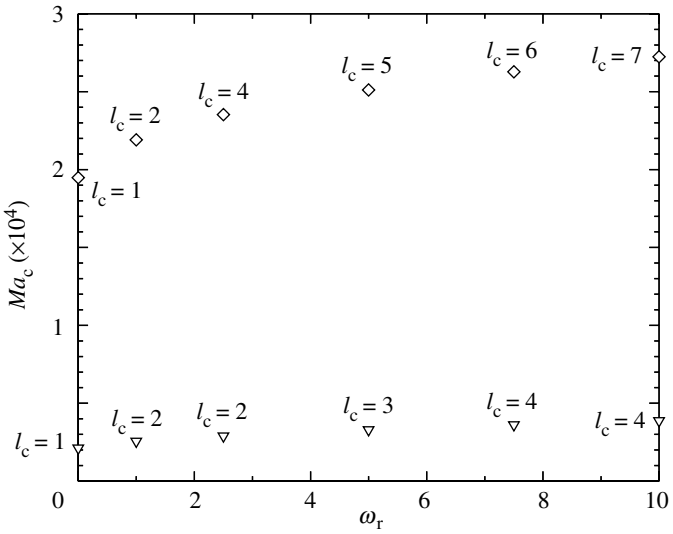

Figure 5. Critical Marangoni number as a function of disturbance growth rate for an octane droplet with a non-deformable free surface at $T_0 = 293$ K ($\Diamond$, $\tau = 0.0001$; $\triangledown$, $\tau = 0.001$).

Table 4. *Variations of Ma_c and l_c with time, τ, and the initial temperature, T_0, of an octane and a heptane droplet*

		octane		heptane	
T_0	τ	Ma_c	l_c	Ma_c	l_c
293	0.0001	19 418.05	1	20 574.69	1
293	0.0005	4 083.96	1	4 329.72	1
293	0.001	2 120.53	1	2 249.14	1
293	0.0015	1 455.58	1	1 544.39	1
313	0.0001	21 058.98	2	22 570.42	2
313	0.0005	4 458.47	1	4 933.07	2
313	0.001	2 316.71	1	2 607.65	1
313	0.0015	1 591.08	1	1 791.91	1
333	0.0001	23 124.78	2	25 413.25	4
333	0.0005	5 056.46	2	5 785.68	2
333	0.001	2 701.93	2	3 095.47	2
333	0.0015	1 865.84	1	2 173.66	2
353	0.0001	25 835.06	4	30 540.23	6
353	0.0005	5 915.52	3	7 411.96	4
353	0.001	3 183.19	2	4 124.19	3
353	0.0015	2235.92	2	2 951.98	3

differences become smaller and smaller as time proceeds. Therefore, the quasi-steady approximation employed in this study will give better and better prediction as time proceeds.

The variations of the critical Marangoni number, Ma_c, versus the initial temperature, T_0, of an octane droplet with three specified disturbance growth rates ($\omega_r = 0$,

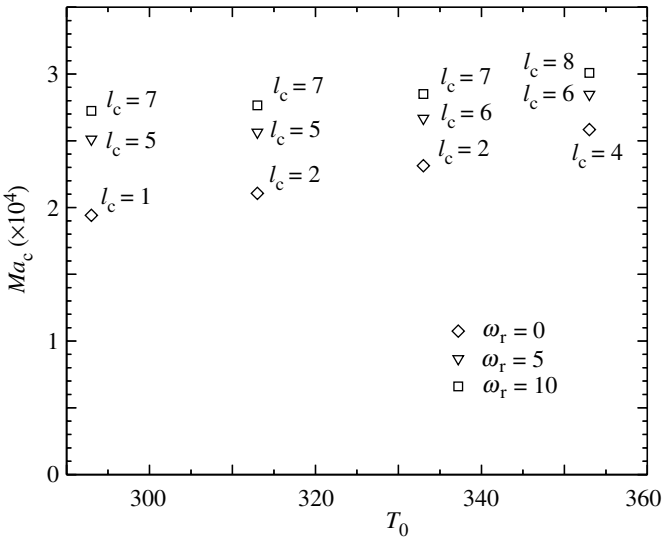

Figure 6. Critical Marangoni number Ma_c versus initial temperature T_0 for an octane droplet with three specified disturbance growth rates; $\tau = 0.0001$.

5 and 10) are shown in figure 6. The corresponding critical wavenumbers, l_c, are also indicated in the figure. It can be seen that, although the values of Ma_c and l_c are different for each disturbance growth rate, they all increase with the droplet initial temperature T_0.

Although the linear stability analysis with a temporarily frozen temperature distribution of the droplet is appropriate for large disturbance growth rates (e.g. $\omega_r \geqslant 10$), the results shown in figures 4, 5 and 6 indicate clearly that the variations of Ma_c and l_c versus time or the droplet initial temperature are all qualitatively similar for small disturbances with different growth rates. Therefore, certain essential physics about the onset of Marangoni instability of an evaporating droplet could be explored by studying the marginal or neutral instability wherein the expression of Ma_c in terms of the droplet initial temperature and the evaporating effect are derived analytically, i.e. equation (4.31). Consequently, a detailed investigation about the marginal or neutral instability will give a direct understanding of the physical mechanism for the onset of Marangoni instability of an evaporating droplet. The following statements, based on equation (4.31), thus serve this purpose.

The onset Marangoni number of neutral instability versus the wavenumbers of small disturbances for four specified initial temperatures of an octane droplet are plotted in figure 7. In each figure, the instability curves for a 'frozen' temperature distribution of the droplet at four specified instants are shown for comparison. The following results can be obtained from these figures.

(1) As time proceeds and evaporation continues, the temperature reduction near the free surface increases, which, together with the consequent variation in surface tension due to disturbances, makes the droplet unstable. As a result, the critical Marangoni number decreases and, hence, the droplet becomes more unstable as time proceeds. As an example, the critical Marangoni number, as a function of dimensionless time for an octane droplet at two different initial temperatures, i.e. $T_0 = 293$ and 353 K, are shown in figure 8. It also can be

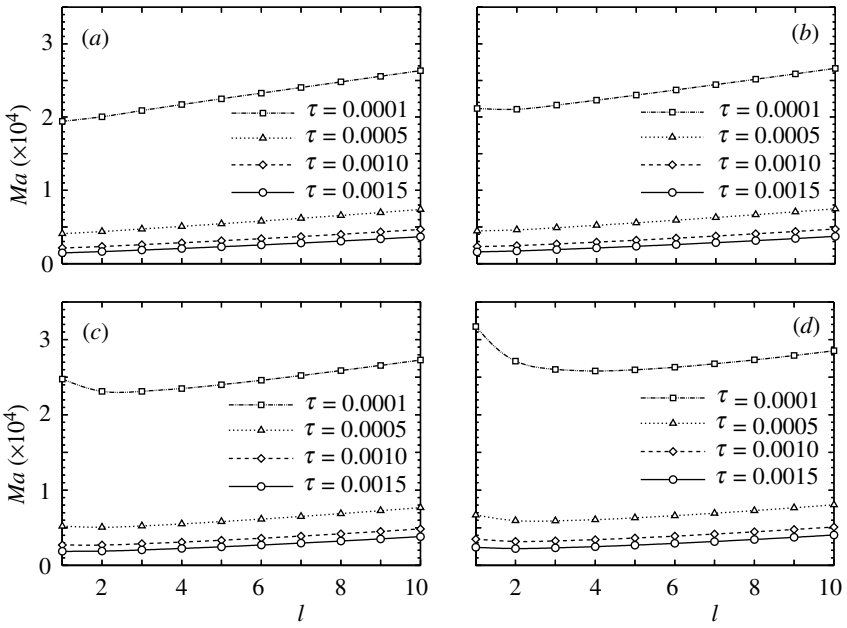

Figure 7. Onset Marangoni number of neutral instability as a function of wavenumber for a non-deformable octane droplet at various instants: (*a*) $T_0 = 293$ K; (*b*) $T_0 = 313$ K; (*c*) $T_0 = 333$ K; (*d*) $T_0 = 353$ K.

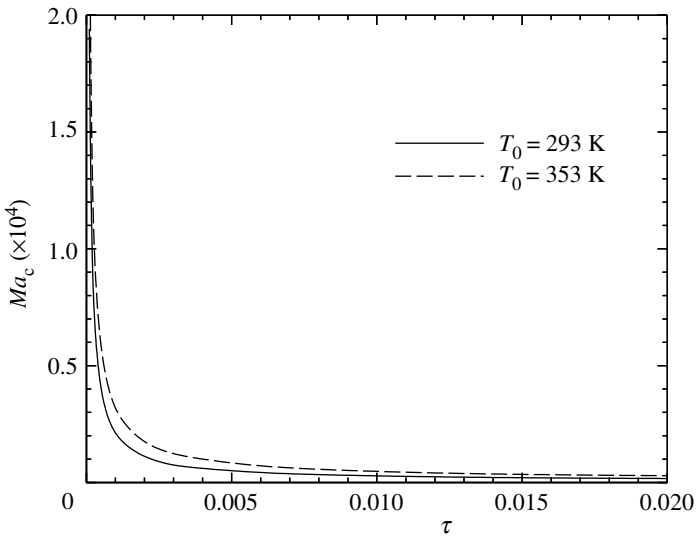

Figure 8. Critical Marangoni number of stationary instability as a function of time for an octane droplet with a non-deformable free surface at two different initial temperatures.

learned from figure 8 that the critical Marangoni number decreases rapidly before $\tau \approx 0.002$, due to great surface temperature reduction within that time-interval. After $\tau \approx 0.002$, Ma_c varies slightly as time proceeds. Similar results were also observed in the planar layer (Ha 1998; Ha & Lai 1998).

(2) When the initial temperature of the droplet, T_0, is less than 293 K, the onset of instability is mostly incurred by the disturbances with a wavenumber of unity. If T_0 is greater than 293 K, the most unstable mode of disturbances might occurs at a higher wavenumber, called the critical wavenumber and denoted by l_c. However, as time proceeds and, meanwhile, the thermal boundary layer thickness grows, the most unstable mode of disturbances tends to shift back to that with a lower wavenumber. The numerically calculated values of Ma_c and l_c for an octane droplet at different initial temperatures and specified instants are given in table 4.

(3) The critical Marangoni number increases with the droplet initial temperature. That is, with a higher initial temperature, the droplet seems to possess intrinsically a certain potential to damp the disturbances. The mechanism for this phenomenon is not obvious. There are two competing mechanisms determining the onset of instability. As stated previously, the temperature reduction near the free surface is the driving potential for the Marangoni instability. Therefore, with a higher initial temperature, which results in a larger temperature reduction near the free surface, the droplet should become more unstable. However, the heat transfer to the surrounding gas due to evaporation, which increases with initial temperature, tends to smooth the surface temperature disturbances. Therefore, the droplet becomes more stable with a higher initial temperature. The competition between these two mechanisms will finally determine the effect of the initial temperature on the droplet instability. Such an explanation can be realized from (4.31), wherein the onset Marangoni number is expressed explicitly in terms of parameters χ and $\bar{T}$. As stated in the last section, the parameter χ indicates the heat transfer to the surrounding gas phase during the evaporation process and $\bar{T}$ implies, in a sense, the temperature reduction near the free surface due to evaporation. Since the onset Marangoni number increases with χ and decreases with $|\bar{T}|$ as indicated by (4.31), the two competing mechanisms explained above become plainly understandable. However, such a competing mechanism does not exist in the flow situation of a planar layer. As a result, the onset Marangoni number for the stationary instability decreases with the initial temperature of the liquid layer (Ha 1998; Ha & Lai 1998).

For further illustration, figures 9 and 10 show the variations of the onset Marangoni number Ma, χ, $\bar{T}$ and a with respect to the initial temperature T_0 of an octane droplet at two specified instants, $\tau = 0.0001$ and 0.0015. Figure 9 is for wavenumber equal to 1 and figure 10 is for wavenumber equal to 5. As shown in figure 9(i), $\tau = 0.0001$, $\bar{T}$ and a are nearly constant for various initial temperatures. However, χ increases with T_0 and so does Ma according to (4.31). This result indicates that, at a fixed instant, the higher initial temperature makes Ma larger through heat transfer effect to the surrounding gas phase. At $\tau = 0.0015$, figure 9 (ii) shows that the variations of χ and a are almost the same as those at $\tau = 0.0001$. However, $|\bar{T}|$ becomes much larger, which implies a larger temperature reduction near the free surface. The onset Marangoni number Ma therefore possesses a lower value than that at $\tau = 0.0001$, according to (4.31). This is exactly the phenomenon illustrated in (1) above, i.e. the droplet becomes more unstable as time proceeds. Similar results can also be obtained for $l = 5$ from figure 10, except that the variation of Ma with

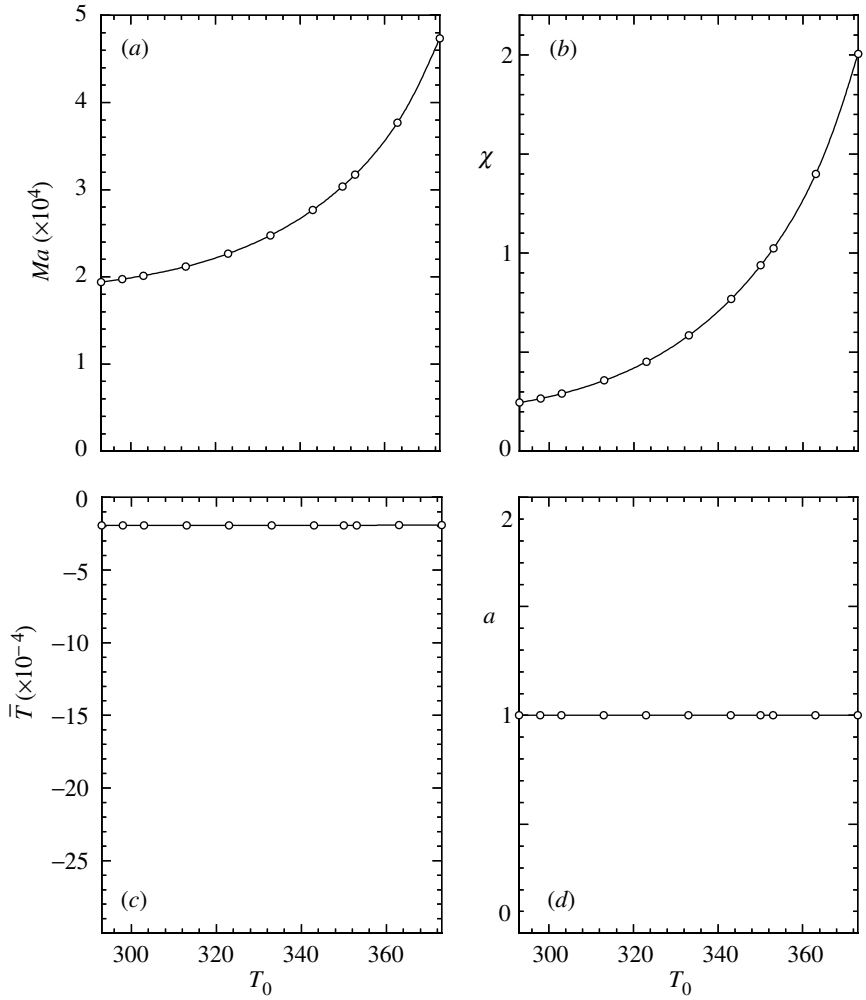

Figure 9. (i) (*a*) Onset Marangoni number, (*b*) dimensionless parameter χ, (*c*) integration $\bar{T}$ and (*d*) constant a versus initial temperatures T_0 for wavenumber $l = 1$ at $\tau = 0.0001$ for a non-deformable octane droplet.

respect to T_0 is much milder than that for $l = 1$. In summary, the variation of the onset Marangoni number with respect to the droplet initial temperature is mainly a function of χ for each specified instant, while, as time proceeds, it becomes mainly affected by $\bar{T}$.

6. Conclusions

The onset of Marangoni instability of a motionless evaporating droplet surrounded by a passive gas is studied theoretically. Under the quasi-steady approximation (which means that the size change of the droplet is negligible), the surrounding gas motion is asymptotically steady, and the temperature distribution of the droplet is temporarily frozen at each specified instant of interest. The linear stability analysis is then applied

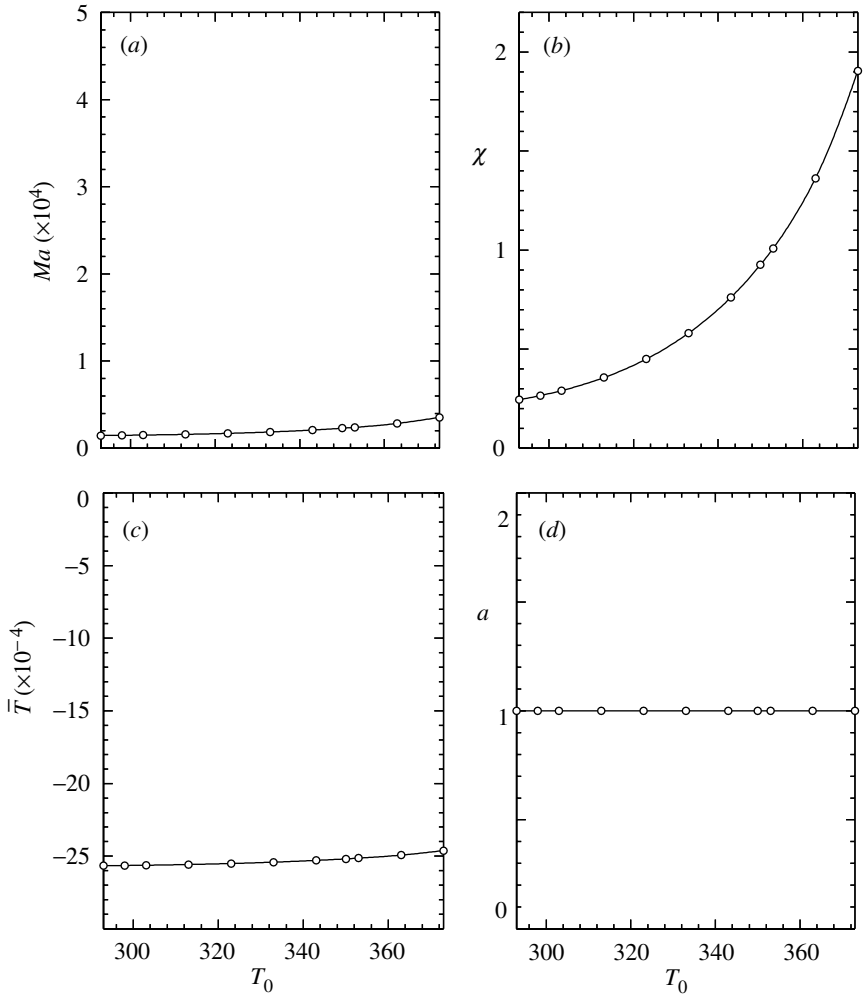

Figure 9. (ii) (*a*) Onset Marangoni number, (*b*) dimensionless parameter χ, (*c*) integration $\bar{T}$ and (*d*) constant a versus initial temperatures T_0 for wavenumber $l = 1$ at $\tau = 0.0015$ for a non-deformable octane droplet.

to obtain a lower limit for Marangoni instability. The following conclusions are drawn from the present study.

(1) The variations of the critical Marangoni number and the critical wavenumber with regard to time or initial temperature are qualitatively similar for small disturbances with different growth rates.

(2) The critical Marangoni numbers for the onset of instability due to small disturbances with different growth rates are of the same order of magnitude.

(3) As time proceeds, the temperature reduction and thermal boundary larger thickness near the free surface become larger and the droplet becomes more unstable.

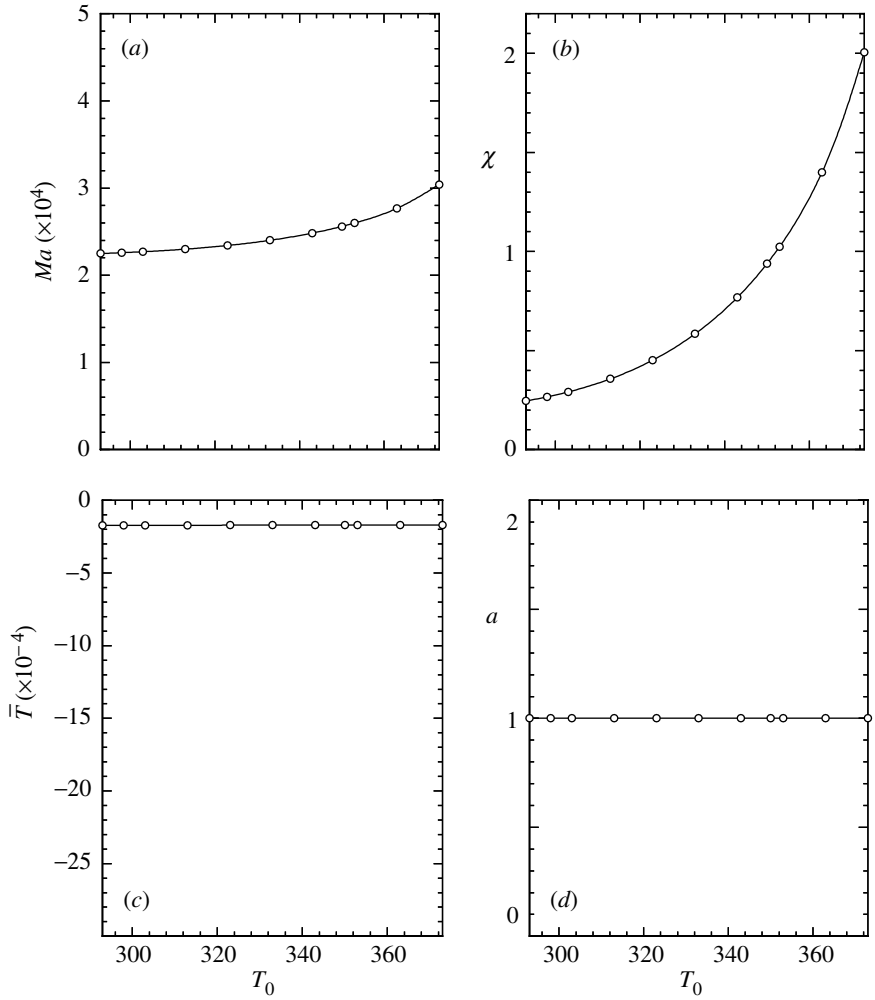

Figure 10. (i) (*a*) Onset Marangoni number, (*b*) dimensionless parameter χ, (*c*) integration $\bar{T}$ and (*d*) constant a versus initial temperatures T_0 for wavenumber $l = 5$ at $\tau = 0.0001$ for a non-deformable octane droplet.

(4) The critical wavenumber of small disturbances for the onset of Marangoni instability increases with the droplet initial temperature.

(5) The onset condition is a strong function of the droplet initial temperature with which the critical Marangoni number increases.

However, only an undeformable free surface with stationary instabilities is considered in the present study. In reality, the free surface is deformable and is usually coupled with the fluid motion. As a result, oscillatory instabilities are expect to occur. Moreover, the time evolution of small disturbances, along with the unsteady temperature variation of the droplet, is also very important and interesting. All of these will be the future work of interest. The present study, which gives a direct understanding of the physical mechanism for the onset of Marangoni instability of an evaporating droplet, shall thus provide a solid foundation for such a further investigation.

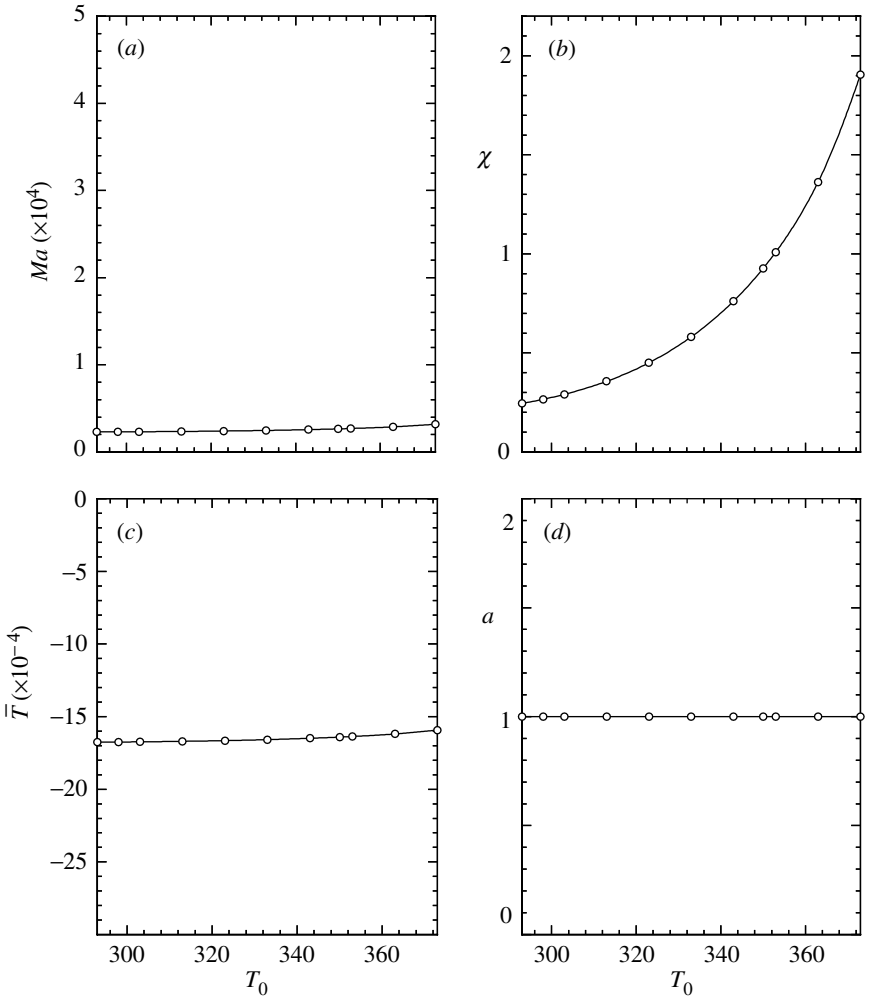

Figure 10. (ii) (*a*) Onset Marangoni number, (*b*) dimensionless parameter χ, (*c*) integration $\bar{T}$ and (*d*) constant a versus initial temperatures T_0 for wavenumber $l = 5$ at $\tau = 0.0015$ for a non-deformable octane droplet.

References

Aharon, I. & Shaw, B. D. 1995 Marangoni instability of bi-component droplet gasification in reduced gravity. In *The 1995 Fall Meeting of the Western States Section of the Combustion Institute*. Stanford, CA: Stanford University.

Aharon, I. & Shaw, B. D. 1996 Marangoni instability of bi-component droplet gasification. *Phys. Fluids* **8**, 1820–1827.

Block, M. J. 1956 Surface tension as the cause of Benard cells and surface deformation in a liquid film. *Nature* **178**, 650–651.

Chandrasekhar, S. 1961 *Hydrodynamic and hydromagnetic stability*, pp. 220–271. Oxford University Press.

Chen, C. F. & Kirchner, R. P. 1971 Stability of time-dependent rotational Couette flow. Part 2. Stability analysis. *J. Fluid Mech.* **48**, 365–384.

Cloot, A. & Lebon G. 1990*a* Surface deformation effect on Marangoni convection in a spherical shell. *Microgravity Sci. Technol.* **3**, 44–46.

Cloot, A. & Lebon G. 1990*b* Marangoni convection in a rotating spherical geometry. *Phys. Fluids* A **2**, 525–529.

Daubert, T. E. & Danner, R. P. 1985 *Data compilation tables of properties of pure compounds.* New York: Design Institute for Physical Property Data, American Institute of Chemical Engineers.

Davis, S. H. 1969 Buoyancy-surface tension instability by the method of energy. *J. Fluid Mech.* **39**, 347–359.

Davis, S. H. 1970 Finite amplitude instability of time-dependent flows. *J. Fluid Mech.* **45**, 33–48.

Dijkstra, H. A. & van de Vooren, A. I. 1985 Initial flow development due to Marangoni convection in a mass transfer system. *Int. J. Heat Mass Transfer* **28**, 2315–2322.

Gogos, G. & Ayyaswamy, P. S. 1988 A model for the evaporation of a slowly moving droplet. *Combust. Flame* **74**, 111–129.

Ha, V. M. 1998 The analysis of Marangoni instability of evaporating liquid. PhD thesis, Department of Mechanical Engineering, National Taiwan University.

Ha, V. M. & Lai, C. L. 1998 Study of Marangoni instability of an evaporating liquid layer. *J. Chin. Inst. Engng* **21**, 547–562.

Hoefsloot, H. C. J. & Hoogstraten, H. W. 1989 Marangoni instability in spherical shells. *Appl. Microgravity Technol.* **2**, 106–108.

Hoefsloot, H. C. J., Hoogstraten, H. W. & Janssen, L. P. B. M. 1990*a* Marangoni instability in a liquid layer bounded by two coaxial cylinder surfaces. *Appl. Sci. Res.* **47**, 1–21.

Hoefsloot, H. C. J., Hoogstraten, H. W. & Janssen, L. P. B. M. 1990*b* Marangoni instability in a liquid layer confined between two concentric spherical surfaces under zero-gravity conditions. *Appl. Sci. Res.* **47**, 357–377.

Hoefsloot, H. C. J., Hoogstraten, H. W., Janssen, L. P. B. M. & Knobbe, J. W. 1992 Growth factors for Marangoni instability in a spherical liquid layer under zero-gravity conditions. *Appl. Sci. Res.* **49**, 161–173.

Homsy, G. M. 1973 Global stability of time-dependent flows: impulsively heated or cooled fluid layers. *J. Fluid Mech.* **60**, 129–139.

Kerr, O. S. 1989 Heating a salinity gradient from a vertical sidewall: linear theory. *J. Fluid Mech.* **207**, 323–352.

Lebon, G., Dauby, P. C. & Cloot, A. 1992 Some problem raised by Marangoni instability in spherical geometry. In *Microgravity fluid dynamics* (ed. H. J. Rath), pp. 71–79. Springer.

Lozinski, D. & Matalon, M. 1993 Thermocapillary motion in a spinning vaporizing droplet. *Phys. Fluids* A **5**, 1596–1601.

McTaggart, C. L. 1984 On the stabilizing effect of surface films in Benard convection. *PCH PhysicoChem. Hydrodyn.* **5**, 321–331.

Mahler, E. G., Schechter, R. S. & Wissler, E. H. 1968 Stability of a fluid layer with time-dependent density gradients. *Phys. Fluids* **11**, 1901–1912.

Neitzel, G. P. 1982 Onset of convection in impulsively heated or cooled fluid layers. *Phys. Fluids* **25**, 210–211.

Niazmand, B. D., Shaw, H. A., Dwyer, H. A. & Aharaon, I. 1995 Effects of Marangoni convection on transient droplet evaporation. *Combust. Sci. Technol.* **103**, 219–233.

Nield, D. A. 1964 Surface tension and buoyancy effects in cellular convection. *J. Fluid Mech.* **19**, 341–352.

Payne, L. E., Song, J. C. & Straughan, B. 1988 Double diffusive porous penetrative convection—thawing subsea permafrost. *Int. J. Engng Sci.* **26**, 797–809.

Pearson, J. R. A. 1958 On convection cells induced by surface tension. *J. Fluid Mech.* **4**, 489–500.

Pirotte, O. & Lebon, G. 1988 Surface-tension driven instability in spherical shells. *Appl. Microgravity Technol.* **1**, 175–179.

Rednikov, A. Ye., Kourdiumov, V. N., Ryazantsev, Yu. S. & Velarde, M. G. 1995 The role of time-varying gravity on motion of a drop induced by Marangoni instability. *Phys. Fluids* **7**, 2670–2678.

Scriven, L. E. & Sternling C. V. 1964 On cellular convection driven by surface-tension gradients: effects of mean surface tension and surface viscosity. *J. Fluid Mech.* **19**, 321–340.

Shih, A. T. & Megaridis, C. M. 1996 Thermocapillary flow effects on convective droplet evaporation. *Int. J. Heat Mass Transfer* **39**, 247–257.

Smith, K. A. 1966 On convective instability induced by surface-tension gradients. *J. Fluid Mech.* **24**, 401–414.

Sternling, C. V. & Scriven, L. E. 1959 Interfacial turbulence: hydrodynamic instability and the Marangoni effect. *AIChE J.* **5**, 514–523.

Vidal, A. & Acrivos, A. 1966 Nature of the neutral state in surface tension driven convection. *Phys. Fluids* **9**, 615–616.

Wahal, S. & Bose, A. 1988 Rayleigh–Benard and interfacial instabilities in two immiscible liquid layers. *Phys. Fluids* **31**, 3502–3510.

Wilson, S. K. 1994 The onset of steady Marangoni convection in a spherical geometry. *J. Engng Math.* **28**, 427–445.

Zeren, R. W. & Reynolds, W. C. 1972 Thermal instabilities in two-fluid horizontal layers. *J. Fluid Mech.* **53**, 305–327.